

Syntheses, Crystal Structure, and Magnetic Properties of Mn_{12} Single-Molecule Magnets with Naphthalenecarboxylate Bridges, $[Mn_{12}O_{12}(O_2CC_{10}H_7)_{16}(H_2O)_4]$ and Their Tetraphenylphosphonium Salts

Guo-Qing Bian, Takayoshi Kuroda-Sowa,* Tadahiro Nogami, Kunihisa Sugimoto,[1] Masahiko Maekawa, Megumu Munakata, Hitoshi Miyasaka,[2] and Masahiro Yamashita[2]

Department of Chemistry, Faculty of Science and Engineering, Kinki University, Higashi-Osaka, Osaka 577-8502

[1]Rigaku Corporation, 3-9-12 Matsubara-cho, Akishima, Tokyo 196-8666

[2]Department of Chemistry, Faculty of Science, Tokyo Metropolitan University, Minami-Osawa, Hachioji, Tokyo 192-0397

Received September 14, 2004; E-mail: kuroda@chem.kindai.ac.jp

The preparation and physical characterization are reported for three Mn_{12} single-molecule magnets (SMMs) having naphthalenecarboxylate bridges, $[Mn_{12}O_{12}(2\text{-nc})_{16}(H_2O)_4]$ (**1**, 2-ncH = 2-naphthalenecarboxylic acid), its Ph_4P^+ salt (**2**) and $[Mn_{12}O_{12}(1\text{-nc})_{16}(H_2O)_4]$ (**3**, 1-ncH = 1-naphthalenecarboxylic acid). Complex $\mathbf{1}\cdot 2CH_2Cl_2\cdot 4.5H_2O$ crystallizes in the monoclinic space group $C2/c$, with cell dimensions at -160 °C of $a = 28.524$ Å, $b = 17.819$ Å, $c = 36.058$ Å, $\beta = 92.399°$, and $Z = 4$. The X-ray structure analysis of $\mathbf{1}\cdot 2CH_2Cl_2\cdot 4.5H_2O$ reveals that each $[Mn_{12}]$ molecule is connected to the neighboring molecules through eight $\pi\cdots\pi$ interactions to form a two-dimensional structure within the *bc*-plane. This is the first SMM that self-assembles two-dimensionally via $\pi\cdots\pi$ interaction. From Arrhenius plots of the frequency dependence of the temperatures of the χ''_M peaks, the effective energy barriers U_{eff} for the reversal of the magnetization spin were estimated to be 61 K, 53 K, and 61 K for high-temperature phases of **1**–**3**, respectively, and 31 K and 33 K for the low-temperature (LT) phases of **1** and **3**, respectively. The analysis of the reduced magnetization data suggests that the LT phase of **1** has an $S = 9$ ground state with $g = 1.998$ and $D = -0.61$ K.

In the ten years since the first discovery of the superparamagnetic behavior of $[Mn_{12}O_{12}(OAc)_{16}(H_2O)_4]$ (Mn_{12}-ac) with a relatively high blocking temperature in 1993,[1] there has been great interest in trying to understand this new magnetic phenomena of so-called single-molecule magnet (SMM). Although there are many efforts to find new SMM's,[2–4] the $[Mn_{12}O_{12}(O_2CR)_{16}(H_2O)_4]$ (R = Me, Et, CH_2Cl, CF_3, Ph et al.) family still possesses the best structural and electronic properties for showing single-molecular magnetic behavior at the highest temperature, and the materials have received a great deal of attention.

It is well-known that the bridging $CH_3CO_2^-$ ligands of Mn_{12}-ac can be replaced by other carboxylates, such as substituted acetates or substituted benzoate, to afford various $[Mn_{12}]$ derivatives.[5–7] However, those carboxylates have no functional groups to coordinate to other metal ions except for the bridging CO_2^- group. If the carboxylate ligands have additional functional groups either to coordinate to other metal ions or to self-assemble via molecular interaction, we can assemble them through the coordination bonds or interactions to form dimers, oligomers, and/or supramolecules of $[Mn_{12}]$ complexes. Recently, Christou et al. reported a dimer of SMM, $[Mn_4O_3Cl_4(O_2CEt)_3(py)_3]_2$, where each $[Mn_4]$ SMM is weakly connected via both six C–H···Cl hydrogen bonds and a Cl···Cl approach.[8] $(PPh_4)[Mn_{12}O_{12}(O_2CC_4H_3S)_{16}(H_2O)_2]$ was reported recently by our group, which shows some S···C or S···S contacts.[9,10] On the basis of our knowledge to date, there are no reports about $[Mn_{12}]$ that show $\pi\cdots\pi$ interaction and self-assembled one or two-dimensional structure. If molecules can self-assemble to supramolecular compounds through various kinds of molecular interactions, for example hydrogen bonds, short contacts and $\pi\cdots\pi$ interactions, we can employ supermolecular chemistry to modulate the quantum physics of SMMs, and can provide a realistic method for fine-tuning the properties of these molecular nanoscale materials.[8] We chose naphthalenecarboxylic acid for this purpose, since it possesses an extended π-conjugated system. Here, we report the syntheses and magnetic susceptibilities of three $[Mn_{12}]$ complexes **1**–**3** that have naphthalenecarboxylate bridges. **1** has been structurally characterized, and it demonstrates an unusual structure, which self-assembles a two-dimensional supramolecule via $\pi\cdots\pi$ interactions of aromatic rings.

Experimental

All chemicals and solvents were used as received. All preparations and manipulations were performed under argon atmosphere using Schlenk techniques. The Mn_{12}-ac was prepared by the literature method.[11]

$[Mn_{12}O_{12}(2\text{-nc})_{16}(H_2O)_4]\cdot 2CH_2Cl_2\cdot 4.5H_2O$ ($\mathbf{1}\cdot 2CH_2Cl_2\cdot 4.5H_2O$). To a slurry of Mn_{12}-ac (200 mg, 0.097 mmol) in

Published on the web June 6, 2005; DOI 10.1246/bcsj.78.1032

CH_2Cl_2 (80 mL) was added a large excess of 2-naphthalenecarboxylic acid (2-ncH, 0.55 g, 3.19 mmol). The mixture was stirred overnight in a closed flask and then the solution was evaporated to dryness. To the residue was added CH_2Cl_2 (80 mL). This solution was stirred for 4 hours and filtered to remove any undissolved solid. Hexane was added to the filtrate until precipitation of a dark brown solid was observed. The resulting solid was collected by filtration and the above treatment was repeated twice to ensure the substitution reaction. Brown plate crystals of **1**·$2CH_2Cl_2$·$4.5H_2O$ suitable for X-ray analysis were obtained from CH_2Cl_2/hexane. The yield was 320 mg (90%). Anal. Calcd for **1** after dry ($C_{176}H_{120}O_{48}Mn_{12}$): C, 57.72; H, 3.30%. Found: C, 57.69; H, 3.98%. Selected IR data (KBr pellet, cm^{-1}): 3421(w), 3057(w), 1599(m), 1556(m), 1467(m), 1413(s), 1337(m), 783(m), 639(m), 604(m), 550(m).

(PPh_4)[$Mn_{12}O_{12}$(2-nc)$_{16}$(H_2O)$_4$] (2). To a stirred dark brown solution of complex **1** (300 mg, 0.082 mmol) in CH_2Cl_2 (20 mL) was added solid PPh_4I (38.5 mg, 0.082 mmol). This solution was stirred for 45 min. The resultant solution was filtered to remove any undissolved solid. To the filtrate a mixture of CH_2Cl_2/hexane and pure hexane were successively added slowly. After three days, black microcrystals were collected by filtration and dried in vacuo. The yield was 290 mg (88%). Anal. Calcd for **2** ($C_{200}H_{140}O_{48}PMn_{12}$): C, 60.03; H, 3.53%. Found: C, 59.95; H, 3.83%. Selected IR data (KBr pellet, cm^{-1}): 3421(w), 3057(w), 1599(m), 1556(m), 1467(m), 1413(s), 1344(m), 785(m), 638(m), 603(m), 552(m).

[$Mn_{12}O_{12}$(1-nc)$_{16}$(H_2O)$_4$] (3). A method similar to that used for the synthesis of **1** was employed but using 1-naphthalenecarboxylic acid (1-ncH). Recrystallization from CH_2Cl_2/hexane gave black block microcrystals. The yield was 97%. Anal. Calcd for **3** ($C_{176}H_{120}O_{48}Mn_{12}$): C, 57.72; H, 3.30%. Found: C, 57.53; H, 3.63%.

Physicochemical Measurements. Direct current (dc) and alternating current (ac) magnetic susceptibility data were collected on microcrystalline or a single-crystal sample restrained in eicosane to prevent torquing on a Quantum Design MPMS2 or MPMS7 SQUID magnetometer equipped with a 1 T or 7 T magnet and capable of achieving temperatures of 1.7 to 400 K. A diamagnetic correction to the observed susceptibilities was applied using Pascal's constants. The magnitude of a.c. field was fixed to 0.3 mT, oscillating at a frequency in the range of 5–997 Hz. Electrochemical studies were performed under argon using an ALS Electrochemical Analyzer (Model 612A) and a standard three-electrodes method (glassy carbon working, Pt wire counter, and Ag/Ag^+/CH_2Cl_2/TBAP reference) with 0.1 M $^nBu_4NPF_6$ as supporting electrolyte. Quoted potentials are vs the ferrocene/ferrocenium couple, used as an external standard. The scan rate for cyclic voltammetry (CV) and the sensitivity were 100 mV/s and 5×10^{-6} A/V, respectively. Distilled solvents were employed; the concentrations of complexes were approximately 1 mM. Infrared spectra were recorded on KBr pellets using a JASCO FT/IR-430 spectrophotometer.

X-ray Structure Analysis. Diffraction data for **1**·$2CH_2Cl_2$·$4.5H_2O$ was collected at −160.1 °C on a Rigaku/MSC Saturn CCD area detector with Rigaku AFC10 diffractometer equipped with graphite monochromated Mo Kα radiation. Crystal data and details of measurements for **1**·$2CH_2Cl_2$·$4.5H_2O$ are summarized in Table 1. The structure was solved by a direct method and expanded using Fourier techniques. The non-hydrogen atoms were refined either anisotropically or isotropically by full-matrix least-squares calculations. Hydrogen atoms were not included. Reliability factors are defined as $R_1 = \Sigma||F_o| - |F_c||/\Sigma|F_o|$ and $wR_2 = [\Sigma w(|F_o| - |F_c|)^2/\Sigma wF_o^2]^{1/2}$. The final R_1 and wR_2 values are 0.092 and 0.236, respectively. Selected bond lengths and angles are listed in Table 2. Microcrystals of complexes **2** and **3** were not single crystals but aggregates of them, and we could not obtain the diffraction data for them. Crystallographic data for **1**·$2CH_2Cl_2$·$4.5H_2O$ have been deposited with the Cambridge Crystallographic Data Centre, CCDC No. 241873. Copies of the data can be obtained free of charge via www:http://www.ccdc.cam.ac.uk (or from the Cambridge Crystallographic Data Centre, 12 Union Road, Cambridge, CB2 1EZ, UK; fax: +44-1233-336033; e-mail: deposit@ccdc.cam.ac.uk).

Table 1. Crystallographic Data for **1**·$2CH_2Cl_2$·$4.5H_2O$

	1·$2CH_2Cl_2$·$4.5H_2O$
Formula	$C_{178}H_{133}Cl_4Mn_{12}O_{52.5}$
Formula Weight	3913.00
Crystal Color, Habit	brown, plate
Crystal Size	$0.20 \times 0.10 \times 0.10$ mm^3
Crystal System	Monoclinic
Space Group	$C2/c$
T (K)	113.1
Unit cell dimensions	
a (Å)	28.524 (4)
b (Å)	17.819 (2)
c (Å)	36.058 (5)
β (°)	92.399 (5)
V (Å^3)	18311.4 (44)
Z	4
D_{calc} (g cm^{-3})	1.412
Diffractometer	Rigaku Saturn/Rigaku AFC10
μ (cm^{-1})	9.34
Radiation, λ (Å)	0.71070
$R_1^{a)}$, $wR^{b)}$	0.092, 0.236
Goodness of Fit Indicator	1.014

a) $R_1 = \Sigma||F_o| - |F_c||/\Sigma|F_o|$ b) $wR_2 = [\Sigma w(|F_o| - |F_c|)^2/\Sigma wF_o^2]^{1/2}$

Results and Discussion

Crystal Structure of [$Mn_{12}O_{12}$(2-nc)$_{16}$(H_2O)$_4$]·$2CH_2Cl_2$·$4.5H_2O$ (1·$2CH_2Cl_2$·$4.5H_2O$). The complex crystallizes in the monoclinic space group $C2/c$, with four formula units in the unit cell. A molecular core structure of **1** is shown in Fig. 1 together with the numbering scheme for some selected atoms. The $[Mn_{12}O_{12}]^{16+}$ moiety is similar to the usual $[Mn_{12}]$ complex except that the four water oxygen atoms bond to Mn1 and Mn7 in 2:2 form. The central cubane structure consists of four Mn^{IV} ions and four μ_3-bridging O^{2-} ions, surrounded by a nonplanar ring of the eight Mn^{III} ions that are bridged by and connected to the cube via eight μ_3-O^{2-} ions. The other coordination sites of manganese ions are occupied by eight axial and eight equatorial μ_2-bridging 2-nc anions and by four water molecules. The structure of **1** has a C_2 axis, which goes through Mn1 and Mn7. Eight peripheral Mn^{III} ions are subjected to Jahn–Teller distortions, which is clearly indicated by the differences in Mn–O bond lengths. Six Mn–O bonds on each Mn^{III} ions are divided into two groups: two long (axial; 2.107–2.240 Å) and four short (equatorial; 1.905–1.985

Table 2. Selected Bond Lengths (Å) and Angles (°) for **1**·$2CH_2Cl_2$·$4.5H_2O$

A	B	Distance (Å)	A	B	Distance (Å)
Mn(1)	O(1)	2.191(8)	Mn(4)	O(13)	1.970(8)
Mn(1)	O(2)	1.891(6)	Mn(4)	O(17)	2.112(7)
Mn(1)	O(9)	1.981(7)	Mn(4)	O(21)	2.128(8)
Mn(2)	Mn(3)	2.783(2)	Mn(5)	Mn(6)	2.775(2)
Mn(2)	O(2)	1.881(6)	Mn(5)	O(6)	1.886(7)
Mn(2)	O(3)	1.883(7)	Mn(5)	O(7)	1.877(7)
Mn(2)	O(10)	1.932(7)	Mn(5)	O(14)	1.927(7)
Mn(2)	O(11)	1.927(7)	Mn(5)	O(15)	1.935(7)
Mn(2)	O(22)	2.184(7)	Mn(5)	O(18)	2.203(7)
Mn(2)	O(24)	2.190(7)	Mn(5)	O(19)	2.203(7)
Mn(3)	O(2)	1.883(7)	Mn(6)	O(4)	1.895(6)
Mn(3)	O(3)	1.875(6)	Mn(6)	O(5)	1.925(7)
Mn(3)	O(4)	1.916(6)	Mn(6)	O(6)	1.839(6)
Mn(3)	O(5)	1.894(6)	Mn(6)	O(7)	1.897(7)
Mn(3)	O(23)	1.921(7)	Mn(6)	O(20)	1.903(7)
Mn(4)	O(3)	1.891(7)	Mn(7)	O(7)	1.875(7)
Mn(4)	O(6)	1.923(6)	Mn(7)	O(8)	2.225(8)
Mn(4)	O(12)	1.997(7)	Mn(7)	O(16)	1.962(8)

A–B–C	Angle (deg)	A–B–C	Angle (deg)
O(1)–Mn(1)–O(2)	92.9(3)	O(6)–Mn(4)–O(13)	93.5(3)
O(1)–Mn(1)–O(9)	90.1(3)	O(6)–Mn(4)–O(17)	93.7(3)
O(2)–Mn(1)–O(9)	92.6(3)	O(6)–Mn(4)–O(21)	89.3(3)
O(2)–Mn(2)–O(3)	83.8(3)	O(12)–Mn(4)–O(13)	79.8(3)
O(2)–Mn(2)–O(10)	94.6(3)	O(12)–Mn(4)–O(17)	87.1(3)
O(2)–Mn(2)–O(11)	176.5(3)	O(12)–Mn(4)–O(21)	89.6(3)
O(2)–Mn(2)–O(22)	93.8(3)	O(13)–Mn(4)–O(17)	90.9(3)
O(2)–Mn(2)–O(24)	83.2(3)	O(13)–Mn(4)–O(21)	85.8(3)
O(3)–Mn(2)–O(10)	176.3(3)	O(17)–Mn(4)–O(21)	175.6(3)
O(3)–Mn(2)–O(11)	97.8(3)	O(6)–Mn(5)–O(7)	83.6(3)
O(3)–Mn(2)–O(22)	93.9(3)	O(6)–Mn(5)–O(14)	97.8(3)
O(3)–Mn(2)–O(24)	86.2(3)	O(6)–Mn(5)–O(15)	179.0(3)
O(10)–Mn(2)–O(11)	83.6(3)	O(6)–Mn(5)–O(18)	91.9(3)
O(10)–Mn(2)–O(22)	90.6(3)	O(6)–Mn(5)–O(19)	85.5(3)
O(10)–Mn(2)–O(24)	90.2(3)	O(7)–Mn(5)–O(14)	174.6(3)
O(11)–Mn(2)–O(22)	89.1(3)	O(7)–Mn(5)–O(18)	91.7(3)
O(11)–Mn(2)–O(24)	93.9(3)	O(7)–Mn(5)–O(19)	84.3(3)
O(22)–Mn(2)–O(24)	176.9(3)	O(7)–Mn(5)–O(15)	95.4(3)
O(2)–Mn(3)–O(3)	84.0(3)	O(14)–Mn(5)–O(15)	83.3(3)
O(2)–Mn(3)–O(4)	172.7(3)	O(14)–Mn(5)–O(18)	93.4(3)
O(2)–Mn(3)–O(5)	89.2(3)	O(14)–Mn(5)–O(19)	90.6(3)
O(2)–Mn(3)–O(23)	91.1(3)	O(15)–Mn(5)–O(18)	88.0(3)
O(3)–Mn(3)–O(4)	97.3(3)	O(15)–Mn(5)–O(19)	94.4(3)
O(3)–Mn(3)–O(5)	90.8(3)	O(18)–Mn(5)–O(19)	175.5(3)
O(3)–Mn(3)–O(23)	93.8(3)	O(4)–Mn(6)–O(5)	83.2(3)
O(4)–Mn(3)–O(5)	83.5(3)	O(4)–Mn(6)–O(6)	91.7(3)
O(4)–Mn(3)–O(23)	96.0(3)	O(4)–Mn(6)–O(7)	88.3(3)
O(5)–Mn(3)–O(23)	174.9(3)	O(4)–Mn(6)–O(20)	175.5(3)
O(3)–Mn(4)–O(6)	91.7(3)	O(5)–Mn(6)–O(6)	96.6(3)
O(3)–Mn(4)–O(12)	95.1(3)	O(5)–Mn(6)–O(7)	171.5(3)
O(3)–Mn(4)–O(13)	174.8(3)	O(5)–Mn(6)–O(20)	96.8(3)
O(3)–Mn(4)–O(17)	89.2(3)	O(6)–Mn(6)–O(7)	84.3(3)
O(3)–Mn(4)–O(21)	89.3(3)	O(6)–Mn(6)–O(20)	92.8(3)
O(6)–Mn(4)–O(12)	173.2(3)	O(7)–Mn(6)–O(20)	91.6(3)

Å) bonds. The axial directions of all Mn^{III} ions are roughly parallel to the molecular z axis defined by the pseudo S_4 axis of the $Mn_{12}O_{12}$ core structure.

The interesting feature of **1**·$2CH_2Cl_2$·$4.5H_2O$ is the existence of the $\pi\cdots\pi$ interaction between equatorial naphthalene rings residing on the neighboring molecules. As can be seen

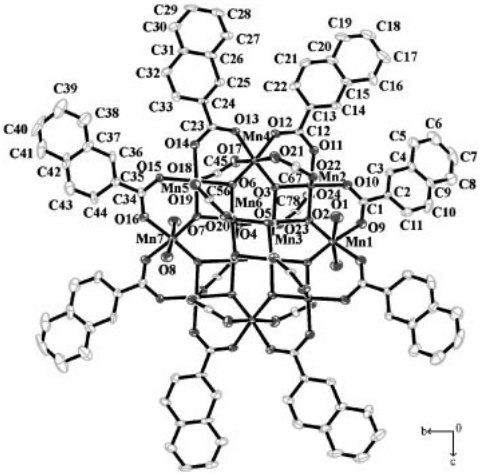

Fig. 1. An ORTEP drawing of a molecular structure of complex **1**·2CH_2Cl_2·4.5H_2O. Since the molecule has a two-fold axis passing through Mn1 and Mn7, the half of the atoms are numbered. Axial naphthalene rings, hydrogen atoms and solvent molecules are omitted for clarity.

from Fig. 2a, each [Mn_{12}] molecule of **1** connects to neighboring four molecules through eight $\pi\cdots\pi$ interactions to form a two-dimensional sheet structure spreading in the *bc* plane. Figures 2b and 2c show side views of $\pi\cdots\pi$ interactions viewed from the *b*- and the *c*-axis, respectively. Naphthalene rings extending to the *c*-axis direction, i.e., those defined by carbon atoms of C13 to C22 and by those of C24 to C33, together with their symmetry-related ones, are almost parallel to each other, with dihedral angles of 0° to 1.4(2)° (Figure 2b). The shortest C···C distance within these naphthalene rings is 3.25(2) Å for C12···C28, although the C12 atom belongs to the carboxylate group connected to the C13 atom. These planes are also parallel to the molecular *xy* plane defined by Mn1, Mn4, Mn7, and Mn4′ (dihedral angles of 7.1(2)–7.8(2)°). On the other hand, among naphthalene rings extending to the *b*-axis direction, the one defined by carbon atoms of C2 to C11 has a large dihedral angle of 31.3(2)° with the molecular *xy* plane, although the other defined by those of C35 to C44 is almost parallel to the molecular *xy* plane (dihedral angle of 7.0(3)°). The shortest C···C distance within these naphthalene rings is 3.34(2) Å for C11···C43 and the dihedral angle between these planes is 24.9(3)° (Figure 2c). As for the inter-layer interaction between two-dimensional sheets, there is no $\pi\cdots\pi$ interaction between inter-molecular axial naphthalene rings.

Recently, weak interactions between SMMs were reported, such as C–H···Cl hydrogen bonds and Cl···Cl approach[8] in [$Mn_4O_3Cl_4(O_2CEt)_3(py)_3]_2$, S···C or S···S contacts[10] in (PPh_4)[$Mn_{12}O_{12}(O_2CC_4H_3S)_{16}(H_2O)_2$]. But no reports are available so far about [Mn_{12}] complexes showing $\pi\cdots\pi$ interaction. Complex **1**·2CH_2Cl_2·4.5H_2O is the first example that molecules self-assemble to a two-dimensional structure through the $\pi\cdots\pi$ interactions. The presence of the $\pi\cdots\pi$ interaction between peripheral naphthalene rings enables each [Mn_{12}] molecule to align in the same direction. Although the influence of these $\pi\cdots\pi$ interactions on the SMM behavior is not clear now, the discovery of the two-dimensional SMMs via $\pi\cdots\pi$ interaction between molecules is important for assembling SMMs to nanoscale magnets.[12]

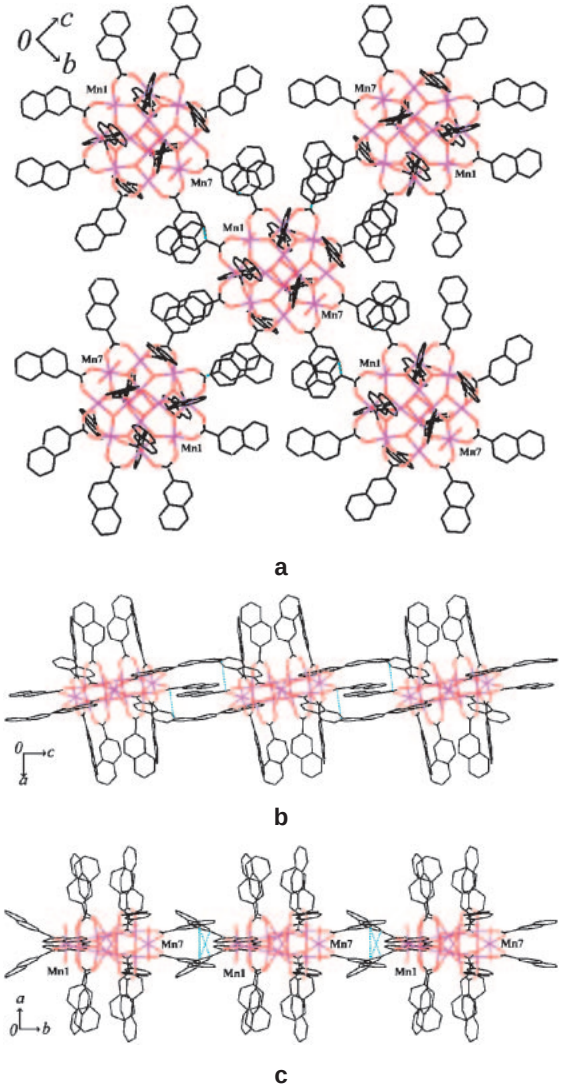

Fig. 2. Two-dimensional strucutre of **1** assembled through π–π interactions between equatorial naphthalene rings. (a): a top view from the *a*-axis, (b) and (c): sideviews from the *b*- and the *c*-axis, respectively. Only Mn1 and Mn7 atoms are labeled for (a) and (c).

Electrochemistry. The Mn_{12} complexes show a rich redox chemistry involving both multiple oxidation and reductions.[6] The cyclic voltammogram (CV) for complex **1** and **2** are shown in Fig. 3. One reversible one-electron oxidation process (0.87/0.73 V vs Fc/Fc^+) and two quasi-reversible one-electron reduction processes (0.21/−0.01 V and −0.11/−0.38 V vs Fc/Fc^+) together with one irreversible reduction process (−0.84 V vs Fc/Fc^+) are observed for complex **1**. The peak separations of these reversible or quasi-reversible processes are 140 mV, 220 mV, and 270 mV, respectively. The relation of each state for **1** is given in Eq. 1, where the voltages indicated are $E_{1/2}$ vs Fc/Fc^+ for the first three processes and a reduction peak potential for the last process. Complex **2**, which contains one-electron reduced [Mn_{12}] compound $\mathbf{1}^-$, shows almost identical redox potentials to those of **1**, except for the zero-bias position. The peak separations of these reversible

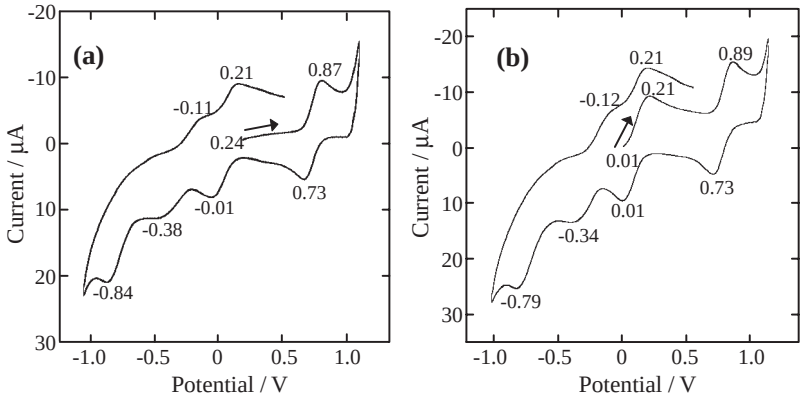

Fig. 3. Cyclic voltammogram of a 1 mM CH_2Cl_2 solution of complex **1** (a) and complex **2** (b) containing 0.1 M (=$(^nBu_4N)(PF_6)$) as supporting electrolyte. The indicated potentials are vs Fc/Fc^+.

or quasi-reversible processes are 160 mV, 200 mV, and 220 mV, respectively.

$$[Mn_{12}]^+ \overset{0.80\ V}{\rightleftharpoons} [Mn_{12}] \overset{0.10\ V}{\rightleftharpoons} [Mn_{12}]^- \overset{-0.25\ V}{\rightleftharpoons} [Mn_{12}]^{2-} \xrightarrow{-0.84\ V} [Mn_{12}]^{3-}, \quad (1)$$

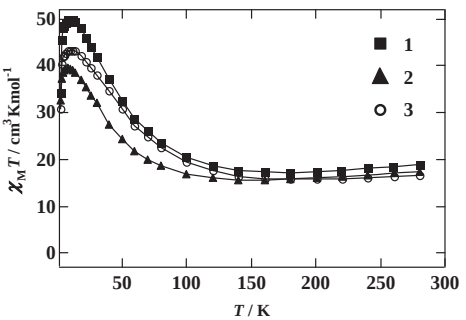

Fig. 4. Plots of $\chi_M T$ vs T for polycrystalline samples of $\mathbf{1}\cdot 2CH_2Cl_2\cdot 4.5H_2O$, **2**, and **3** fixed with eicosane wax.

Dc Magnetic Susceptibility. Solid-state, variable temperature magnetic susceptibility measurements were performed on a freshly prepared polycrystalline sample of complexes **1**–**3**, suspended in eicosane to prevent torquing. Dc magnetic susceptibility (χ_M) data were collected from 2 K to 280 K at 1.0 T magnetic field; the results are shown in Fig. 4. As temperature increased, the $\chi_M T$ value of $\mathbf{1}\cdot 2CH_2Cl_2\cdot 4.5H_2O$ showed a maximum of 50.0 $cm^3\,K\,mol^{-1}$ at 10 K and a broad minimum of 17.2 $cm^3\,K\,mol^{-1}$ at around 180 K and again increases slightly to 18.8 $cm^3\,K\,mol^{-1}$ at 280 K. Similar behaviors were observed for complexes **2** and **3**: a maximum of 39.6 $cm^3\,K\,mol^{-1}$ at around 8 K and a broad minimum of 15.6 $cm^3\,K\,mol^{-1}$ at around 160 K for complex **2** and a maximum of 43.3 $cm^3\,K\,mol^{-1}$ at around 10 K and a broad minimum of 15.7 $cm^3\,K\,mol^{-1}$ at around 200 K for complex **3** were observed.

Ac Magnetic Susceptibility. In order to investigate the dynamic behavior of the magnetic moment, the ac magnetic susceptibility of a freshly prepared microcrystalline sample of $\mathbf{1}\cdot 2CH_2Cl_2\cdot 4.5H_2O$ was measured. Figure 5a shows plots of

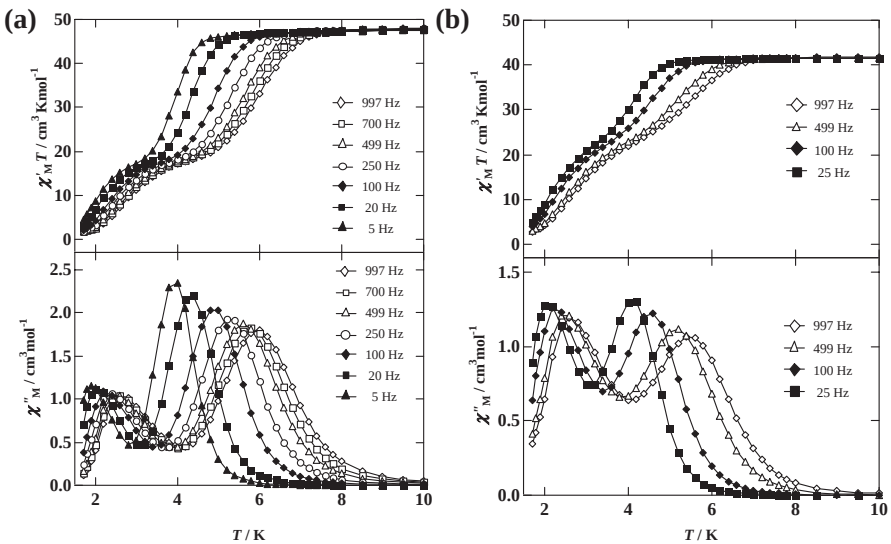

Fig. 5. (a) Plots of $\chi'_M T$ vs T (top) and χ''_M vs T (bottom) for a polycrystalline sample of complex $\mathbf{1}\cdot 2CH_2Cl_2\cdot 4.5H_2O$ in a 0.3 mT ac field oscillating at the indicated frequencies, where χ'_M and χ''_M are the in-phase and the out-of-phase magnetic susceptibilities, respectively. (b) Same as (a) but powder sample of **1** after being dried under reduced pressure for 4 hours was used.

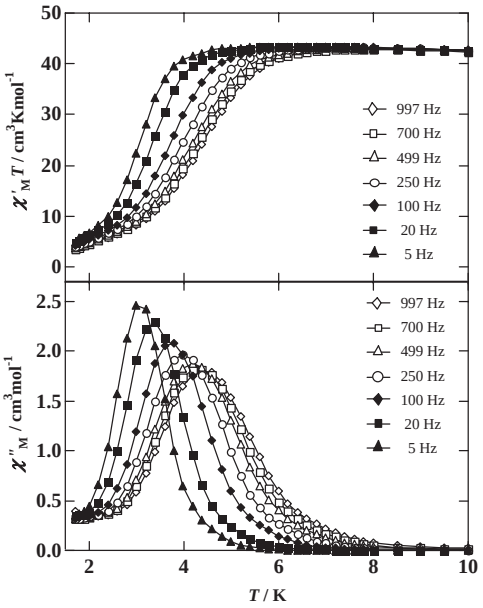

Fig. 6. Plots of $\chi'_{\mathrm{M}}T$ vs T (top) and $\chi''_{\mathrm{M}}T$ vs T (bottom) for a polycrystalline sample of complex **2** in a 0.3 mT ac field oscillating at the indicated frequencies.

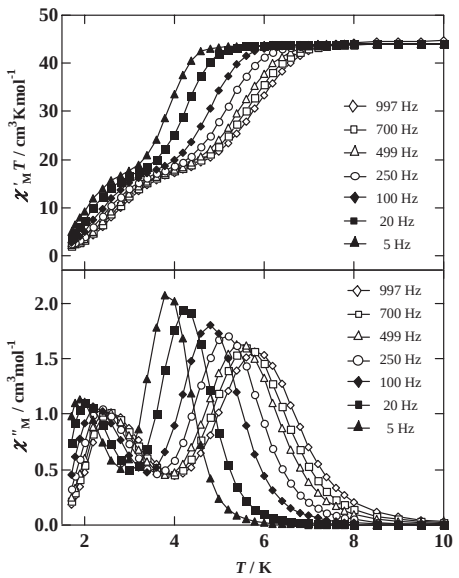

Fig. 7. Plots of $\chi'_{\mathrm{M}}T$ vs T (top) and $\chi''_{\mathrm{M}}T$ vs T (bottom) for a polycrystalline sample of complex **3** in a 0.3 mT ac field oscillating at the indicated frequencies.

$\chi'_{\mathrm{M}}T$ vs T (top) and χ''_{M} vs T (bottom), respectively, where χ'_{M} and χ''_{M} are in-phase and out-of-phase ac susceptibility, respectively. The values for complexes **2** and **3** are also shown in Figs. 6 and 7, respectively. The $\chi'_{\mathrm{M}}T$ values of **1**–**3** at 10 K are 47.0, 43.0, and 44.0 $\mathrm{cm^3\,K\,mol^{-1}}$, respectively. As temperature decreases, these values start to decrease at a certain temperature depending on frequency. The decrease of $\chi'_{\mathrm{M}}T$ value corresponds to the appearance of an out-of-phase signal (χ''_{M}). The χ''_{M} values of **1**·$2CH_2Cl_2$·$4.5H_2O$ showed two peaks for each ac frequency, one in 4–7 K range and the other in 2–3 K range; these are corresponding to the high-temperature (HT) and the low-temperature (LT) phases, respectively, with the former being dominant. Those of **2**, on the other hand, showed only one peak between 2–6 K, which can be assigned to the HT phase of anionic Mn_{12} complex **2**. Those of **3**, just like **1**·$2CH_2Cl_2$·$4.5H_2O$, showed two peaks for each ac frequency, which correspond to the HT and the LT phases, respectively.

In order to investigate the effect of a removal of crystalline solvent on the magnetic properties, the ac magnetic susceptibility of a powder sample of **1**, after being dried in a reduced pressure for 4 hours, was also measured. Figure 5b shows plots of $\chi'_{\mathrm{M}}T$ vs T (top) and χ''_{M} vs T (bottom), respectively. One clear difference between Fig. 5a and Fig. 5b is the relative intensity of HT and LT phases. The intensity of LT phase increased at the sacrifice of that of HT phase. Since the origin of two phases in the χ''_{M}–T plot is ascribed to the presence of two Jahn–Teller isomers,[13,14] it is reasonable to think that the removal of solvent molecules affects the coordination geometry around Mn^{III} ions. A similar phenomenon was also reported in $[Mn_{12}O_{12}(O_2CC_6H_4$-$p$-$Me)_{16}(H_2O)_4]$,[15] where the intensities of the LT phase were drastically increased by changing the crystalline solvent from H_2O to p-MeC_6H_4COOH.

The frequency dependence of the χ''_{M} peak temperature can be analyzed by the Arrhenius law. On the basis of the plots of the natural logarithm of the relaxation time τ evaluated from $1/(2\pi\nu)$, where ν is the ac frequency, versus the inverse of the χ''_{M} peak temperature T, the effective energy barrier U_{eff} and pre-exponential factor τ_0 can be estimated by the following equation:[16]

$$\tau = \tau_0 \exp\left(\frac{U_{\mathrm{eff}}}{k_{\mathrm{B}}T}\right), \tag{2}$$

where k_{B} is the Boltzmann constant. The Arrhenius plots for **1**–**3** are shown in Fig. 8. The solid lines show the results of least-squares fits of the ac susceptibility relaxation data to Eq. 2. The effective energy barrier U_{eff} and pre-exponential factor τ_0 are determined as shown in Table 3. The effective energy barriers U_{eff} for HT phases of **1** to **3** were evaluated to be 61, 53, and 61 K, respectively. These values are somewhat

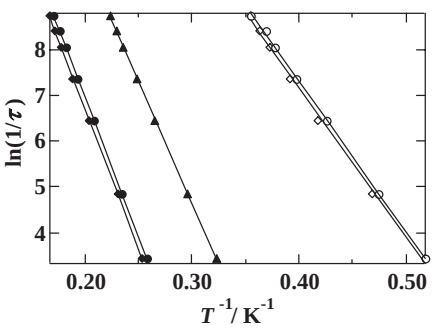

Fig. 8. Plots of the natural logarithm of the inverse of the magnetization relaxation time $\ln(1/\tau)$ vs the inverse of the absolute temperature of χ''_{M} peaks for the **1**·$2CH_2Cl_2$·$4.5H_2O$ (◆,◇), **2** (●,○), and **3** (▲). High-temperature and low-temperature phases are indicated by filled and open symbols, respectively. Solid lines represent least-squares fits of the data to the Arrhenius equation (see the text).

Table 3. Pre-exponential Factor τ_0 and the Effective Energy Barrier U_{eff} from Arrhenius Plots for Complexes **1**·$2CH_2Cl_2$·$4.5H_2O$, **2**, and **3**

Complex	Phase	τ_0/s	U_{eff}/K
1·$2CH_2Cl_2$·$4.5H_2O$	HT	6.0×10^{-9}	61
	LT	1.7×10^{-9}	33
2	HT	1.2×10^{-9}	53
3	HT	4.9×10^{-9}	61
	LT	1.3×10^{-9}	33

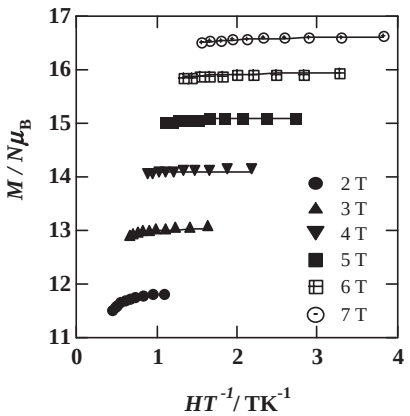

Fig. 9. Reduced magnetization data for **1** with different external field. Lines show the best-fit assuming $S = 9$, $g = 1.998$, and $D = -0.61$ K.

smaller than those obtained for neutral [Mn_{12}] complexes, such as [$Mn_{12}O_{12}(O_2CC_4H_3S)_{16}(H_2O)_4$] (69.1 K[10]) and [$Mn_{12}O_{12}$-$(NO_3)_4(O_2CCH_2Bu^t)_{12}(H_2O)_4$] (72 K[17]). The U_{eff} value of the HT phase of **2** was estimated to be 53 K, which is also smaller than the values for anionic $[Mn_{12}]^-$ SMMs, such as (PPh_4)[$Mn_{12}O_{12}(O_2CEt)_{16}(H_2O)_4$] (60.2 K[18]), ($PPh_4$)-[$Mn_{12}O_{12}(O_2CC_4H_3S)_{16}(H_2O)_2$] (57.1 K[10]) or ($PPh_4$)-[$Mn_{12}O_{12}(O_2CPh)_{16}(H_2O)_4$] (55 K,[19] 57.5 K[20]). At 997 Hz ac frequency, the anionic complex **2** shows χ''_M peak at 4.5 K, while the parent neutral complex **1** shows a χ''_M peak at 6.0 K. The lower temperature shift of the χ''_M peak on one electron reduction has been also observed for other [Mn_{12}] complexes.[7]

Reduced Magnetization. In order to estimate the ground spin state (S) and the magnitude of the zero-field splitting (D) of **1**, the dc magnetization values were determined in the temperature range of 1.9–4.5 K and at external fields of 2.0–7.0 T for finely ground powder sample of complex **1**. The sample was restrained in an eicosane matrix to prevent torquing at high fields. The observed magnetization data $M/(N\mu_B)$ were plotted vs H/T in Fig. 9, which were fitted with a magnetization fitting program "axfit"[21] assuming an $S = 9$ ground state. The lines in Fig. 9 show the fitting with parameters of $g = 1.998$ and $D = -0.61$ K. If we assume an $S = 10$ ground state, a similar fit can be obtained but a g-value of 1.80 is too small compared to typical g-values of 1.95–1.99[3b,6a,22,23,24] for some [Mn_{12}] SMM's. Since the removal of crystalline solvents of **1** increases a LT/HT ratio, as described in the ac magnetization analyses section, the above-mentioned $S = 9$ ground state can

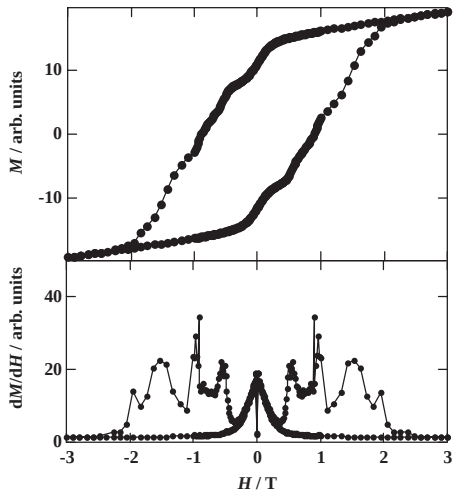

Fig. 10. A magnetization hysteresis loop for oriented crystals of **1**·$2CH_2Cl_2$·$4.5H_2O$ in eicosane matrix measured at 1.9 K (top) and the corresponding first derivatives dM/dH (bottom).

be assigned to the LT phase of **1**. The theoretical energy barrier U ($=S^2|D|$) for a spin flip can be estimated to be 49 K. This value is larger than the U_{eff} of 33 K for the LT phase and is smaller than that for the HT phase (61 K). Since the presence of quantum tunneling of the magnetization leads to a smaller value of U_{eff} than that of U,[25,26,27] the assignment to the LT phase is more reasonable than that to the HT phase. However, HFEPR measurements are needed for a definitive ground-state assignment.

Magnetization Hysteresis Loop. It has been established that Mn_{12} SMMs exhibit magnetization hysteresis loops. Especially for SMM, step-like sudden decreases of magnetization can be also seen, which are attributed to the quantum tunneling of magnetization. In order to observe hysteresis loop of **1**, a 4.62 mg of microcrystalline sample placed in a capsule with eicosane was subjected to a 7.0 T external magnetic field at 325 K, then cooled to fix it in space. Thus, magnetization easy axes of microcrystals should be all aligned to the direction of the external field. The field dependence of the dc magnetization measured at 1.9 K is shown in the top portion of Fig. 10. Although a clear hysteresis loop was observed, the magnetization did not saturate even at 3 T. Since all [Mn_{12}] molecules of **1** have a uniform orientation in a crystal, the reason for this non-saturation behavior is probably the presence of the LT phase whose magnetization easy axis is not parallel to the molecular z-axis. The tilting of the magnetization easy axis about 12° away from the molecular z-axis has been reported for the LT phase of Mn_{12}–benzoate.[15] Since the magnetization relaxation time for the LT and the HT phases of **1** at 1.9 K estimated by using Eq. 2 and τ_0 and U_{eff} in Table 3 are 0.06 s and 5×10^5 s, respectively, it is clear that the hysteresis loop with steps in Fig. 10 is due to the HT phase of **1**. As the field is decreased from +3 T, five steps can be seen between 0 to −1.93 T, with about 0.5 T intervals. They are clearly seen in the first derivative of the magnetization, shown in the bottom portion of Fig. 10. These steps correspond to the quantum tunneling of magnetization between two sublevels of $m_s = S$ and $m_s = -S + n$, where $n = 0$, 1, 2, 3, and 4. Since the condition that

the quantum tunneling occurs can be expressed as Eq. 3, we can estimate $|D| = 0.67$ K for the HT phase by using $\Delta H = 0.5$ T and assuming $g = 2.00$.

$$H_{S,-S+n} = nD/(g\mu_B). \quad (3)$$

Conclusion

We have synthesized three [Mn_{12}] derivatives with naphthalenecarboxylate bridges, **1–3**, which showed SMM behavior in their ac susceptibility. The crystal structure determination of **1** revealed that each molecule is connected to neighbors through four $\pi\cdots\pi$ interactions. Although no direct effect of these $\pi\cdots\pi$ interactions on the magnetic properties of **1** is found, complex **1** is the first two-dimensional [Mn_{12}] complex self-assembled via $\pi\cdots\pi$ interaction between naphthalene rings, which represents not only a useful expansion of this family of SMMs but also the molecular design for potential applications of SMMs.

This work was supported in part by a Grant-in-Aid for Science Research from the Ministry of Education, Science and Culture, Japan. The authors are grateful to Kinki University for its financial support.

References

1 R. Sessoli, D. Gatteschi, A. Caneschi, and M. A. Novak, *Nature*, **365**, 141 (1993).

2 B. Schwarzschild, *Phys. Today*, **1997**, 17.

3 a) J. R. Friedman, M. P. Sarachik, J. Tejada, and R. Ziolo, *Phys. Rev. Lett.*, **76**, 3830 (1996). b) N. E. Chakov, W. Wernsdorfer, K. A. Abboud, D. N. Hendrickson, and G. Christou, *Dalton Trans.*, **2003**, 2243.

4 E. M. Chudnovsky, *Science*, **274**, 938 (1996).

5 R. Sessoli, H.-L. Tsai, A. R. Schake, S. Wang, J. B. Vincent, K. Folting, D. Gatteschi, G. Christou, and D. N. Hendrickson, *J. Am. Chem. Soc.*, **115**, 1804 (1993).

6 a) H. J. Eppley, H.-L. Tsai, N. D. Vries, K. Folting, G. Christou, and D. N. Hendrickson, *J. Am. Chem. Soc.*, **117**, 301 (1995). b) M. Soler, W. Wernsdorfer, K. A. Abboud, J. C. Huffman, E. R. Davidson, D. N. Hendrickson, and G. Christou, *J. Am. Chem. Soc.*, **125**, 3576 (2003).

7 T. Kuroda-Sowa, M. Lam, A. L. Rheingold, C. Frommen, W. M. Reiff, M. Nakano, J. Yoo, A. L. Maniero, L.-C. Brunel, G. Christou, and D. N. Hendrickson, *Inorg. Chem.*, **40**, 6469 (2001).

8 W. Wernsdorfer, N. Aliaga-Alcalde, D. N. Hendrickson, and G. Christou, *Nature*, **416**, 406 (2002).

9 T. Kuroda-Sowa, T. Nogami, M. Maekawa, and M. Munakata, *Mol. Cryst. Liq. Cryst.*, **379**, 179 (2002).

10 T. Kuroda-Sowa, T. Nogami, H. Konaka, M. Maekawa, M. Munakata, H. Miyasaka, and M. Yamashita, *Polyhedron*, **22**, 1795 (2003).

11 T. Lis, *Acta Crystallogr. Sect. B*, **B36**, 2042 (1980).

12 M. N. Leuenberger and D. Loss, *Nature*, **410**, 789 (2001).

13 Z. Sun, D. Ruiz, N. R. Dilley, M. Soler, J. Ribas, K. Folting, M. B. Maple, G. Christou, and D. N. Hendrickson, *Chem. Commun.*, **1999**, 1973.

14 K. Takeda, K. Awaga, T. Inabe, A. Yamaguchi, H. Ishimoto, T. Tomita, H. Mitamura, T. Goto, N. Mori, and H. Nojiri, *Phys. Rev. B*, **65**, 094424 (2002).

15 S. M. J. Aubin, Z. Sun, H. J. Eppley, E. M. Rumberger, I. A. Gunzei, K. Folting, P. K. Ganzel, A. L. Rheingold, G. Christou, and D. N. Hendrickson, *Inorg. Chem.*, **40**, 2127 (2001).

16 S. M. J. Aubin, M. W. Wemple, D. A. Adams, H.-L. Tsai, G. Christou, and D. N. Hendrickson, *J. Am. Chem. Soc.*, **118**, 7746 (1996).

17 P. Artus, C. Boskovic, J. Yoo, W. E. Streib, L.-C. Brunel, D. N. Hendrickson, and G. Christou, *Inorg. Chem.*, **40**, 4199 (2001).

18 S. M. J. Aubin, S. Spagna, H. J. Eppley, R. E. Sager, G. Christou, and D. N. Hendrickson, *Chem. Commun.*, **1998**, 803.

19 K. Takeda and K. Awaga, *Phys. Rev. B*, **56**, 14560 (1997).

20 S. M. J. Aubin, Z, Sun, L. A. Pardi, J. Krzystek, K. Folting, L.-C. Brunel, A. L. Rheingold, G. Christou, and D. N. Hendrickson, *Inorg. Chem.*, **38**, 5329 (1999).

21 J. Yoo, A. Yamaguchi, M. Nakano, J. Krzystek, W. E. Streib, L.-C. Brunel, H. Ishimoto, G. Christou, and D. N. Hendrickson, *Inorg. Chem.*, **40**, 4604 (2001).

22 P. D. W. Boyd, Q. Y. Li, J. B. Vincent, K. Folting, H. R. Chang, W. E. Strieb, J. C. Huffman, G. Christou, and D. N. Hendrickson, *J. Am. Chem. Soc.*, **110**, 8537 (1988).

23 Y. Miyazaki, A. Bhattacharjee, M. Nakano, K. Saito, S. M. J. Aubin, H. J. Eppley, G. Christou, D. N. Hendrickson, and M. Sorai, *Inorg. Chem.*, **40**, 6632 (2001).

24 N. E. Chakov, K. A. Abboud, L. N. Zakharov, A. L. Rheingold, D. N. Hendrickson, and G. Christou, *Polyhedron*, **22**, 1759 (2003).

25 M. A. Novak and R. Sessoli, "Quantum Tunneling of Magnetization-QTM'94," ed by L. Gunther and B. Barbara, Kluwer, Amsterdam (1995), p. 171.

26 J. R. Friedman, M. P. Sarachik, J. Tejada, J. Maciejewski, and R. Ziolo, *J. Appl. Phys.*, **79**, 6031 (1996).

27 J. R. Friedman, M. P. Sarachik, J. Tejada, and R. Ziolo, *Phys. Rev. Lett.*, **76**, 3830 (1996).